Ab initio, VTST, and QCT study of the $1\,^2A''$ potential energy surface of the $N(^2D)+O_2(X\,^3\Sigma_g^-)\rightarrow O(^3P)+NO(X\,^2\Pi)$ reaction

Miguel González,[a] Irene Miquel, and R. Sayós[a]
Departament de Química Física i Centre de Recerca en Química Teòrica, Universitat de Barcelona, C/ Martí i Franquès, 1, 08028 Barcelona, Spain

(Received 30 May 2001; accepted 14 August 2001)

An *ab initio* study based on the CASSCF (Complete Active Space Self-Consistent Field) and CASPT2 (Second-Order Perturbation Theory on a CASSCF wave function) methods has been carried out on the ground $^2A''$ potential energy surface (PES) involved in the relevant atmospheric reaction between $N(^2D)$ and O_2 to produce $O(^3P)$ and NO. Also, some intersections between PES have been studied. The stationary points have been characterized and a grid of more than 800 points have been fitted to an analytical function. This analytical representation of the PES has been used to obtain kinetic and dynamic properties of the reaction. The rate constant of this reaction has been calculated at different levels of theory [variational transition state theory (VTST) and quasiclassical trajectory (QCT) methods] and has been compared with the experimental values (overall rate constant including physical electronic quenching) obtaining a good agreement. The QCT method has also been employed to study the properties of products from both the abstraction and insertion microscopic mechanisms. The vibrational distribution of NO arising from the reaction at 100 K has also been calculated and compared with the experimental ones. In this case, the agreement between the theoretical and the experimental results is not so good, the experimental vibrational distribution being less excited. Future work is necessary to determine the origin of this difference. © *2001 American Institute of Physics.* [DOI: 10.1063/1.1408301]

I. INTRODUCTION

The reactions of electronically excited species like $N(^2D)$ play an important role in atmospheric chemistry, discharges in plasmas, lasers, and photolysis systems.[1] In the upper atmosphere, the deactivation of $N(^2D)$ is mainly due to molecular oxygen in its ground state $O_2(X\,^3\Sigma_g^-)$ to produce vibrationally excited NO. This reaction is the main source of NO observed in the aurora. The reaction between $N(^2D)$ and O_2 can take place by means of two reactive channels:

$$N(^2D)+O_2(X\,^3\Sigma_g^-) \rightarrow O(^1D)+NO(X\,^2\Pi), \Delta H^\circ_{298\,K}=-41.4\ \text{kcal mol}^{-1}, \quad (1)$$

[2,3]

$$\rightarrow O(^3P)+NO(X\,^2\Pi), \Delta H^\circ_{298\,K}=-86.7\ \text{kcal mol}^{-1}. \quad (2)$$

[2,3]

The overall rate constant [reactions (1), (2) and physical electronic quenching] has been measured by several authors[4–16] at low and moderate temperatures (210–465 K) and a global rate constant of $5.2\times10^{-12}\,\text{cm}^3\,\text{molecule}^{-1}\,\text{s}^{-1}$ at 298 K has been recommended.[17]

Recent theoretical papers[1,18] have shown that reaction (2) is strongly dominant over reaction (1), that plays an essentially negligible role in the deactivation of $N(^2D)$ by O_2. There is only one potential energy surface (PES) involved in reaction (1) and its barrier is quite large (about 20 kcal mol^{-1}). Because of this, reaction (1) is not important in overall reactivity. As refers reaction (2), it involves six PES ($2\,^2A'$, $3\,^2A'$, $1\,^2A''$, $2\,^2A''$, $3\,^4A'$ and $3\,^4A''$ PES) and two of them present very low-energy barriers (0.08 and 0.25 kcal mol^{-1} for the $2\,^2A'$ and $1\,^2A''$ PES, respectively[1]). Nevertheless, if we take into account the zero-point energy (ZPE), the energetic requirement is about 0.50 kcal mol^{-1} in both PES. Due to this, reaction (2) is also important in reactivity at low temperatures. From VTST (Variational Transition State Theory) calculations we have reproduced[1] the experimental rate constant of the overall deactivation of $N(^2D)$ by means of O_2 and have also suggested that physical electronic quenching is negligible. Hence, from the calculations it turns out that the formation of NO is mainly due to reaction (2).

Regarding the NO vibrational distribution of reaction (2), it has also been measured,[19] showing an inverted distribution peaking at $NO(v'=7)$ at 100 K. Braunstein and Duff[18] have succeeded in reproducing qualitatively these vibrational distributions by means of a QCT study on the $2\,^2A'$ and $1\,^2A''$ PES but considering a temperature of 500 K.

Recently, we have carried out a detailed study of the $2\,^2A'$ PES implied in reaction (2).[20] In that work we computed more than 600 *ab initio* points that were fitted to an analytical function. We used this PES to perform a QCT kinetic and dynamic study of reaction (2). The experimental populations are peaked at $v'=7$ while our results showed a more excited vibrational distribution. To improve these results and due to the importance of the $1\,^2A''$ PES in reaction

[a]Authors to whom correspondence should be addressed. Electronic mail: miguel@qf.ub.es, r.sayos@qf.ub.es

 © 2001 American Institute of Physics

TABLE I. *Ab initio* CASSCF (17,12) energy barriers (kcal mol^{-1}) for the abstraction transition states on the 2 $^2A'$ and 1 $^2A''$ PES.[a]

Basis set	TS1 2$^2A'$ PES[b]	TS1 1$^2A''$ PES
cc-pVDZ	6.35	6.50
cc-pVTZ	6.65	6.83
cc-pVQZ	6.78	6.97

[a]The calculations have been performed at the optimal cc-pVTZ geometry.
[b]References 1 and 20.

(2), in the present work we have carried out a similar *ab initio*/QCT study of this PES.

This work is organized as follows: In Sec. II the methodology employed in the *ab initio* calculations, the analytical fit of the PES and the evaluation of the rate constants and vibrational distributions is described. In Sec. III we show the results obtained, that is to say, the stationary points and the minimum energy path on the PES, the parameters of the analytical fit and the rate constant and vibrational distributions for the 1 $^2A''$ PES, and in Sec. IV the more relevant conclusions are given.

II. METHODOLOGY

A. *Ab initio* methods

As indicated in Sec. I, several PES (2 $^2A'$, 3 $^2A'$, 1 $^2A''$, 2 $^2A''$, 3 $^4A'$, and 3 $^4A''$ surfaces) connect reactants and products of reaction (2).[1,20] In a previous paper[20] we have performed a detailed *ab initio* study of the 2 $^2A'$ PES. In the present paper we will perform an analogous study on the 1 $^2A''$ PES, as this one along with the 2 $^2A'$ PES are the most involved in the reactivity of N(^2D) and O_2.

The 1 $^2A''$ PES has been studied by means of the same *ab initio* methodology employed in previous papers.[1,20] We have carried out CASSCF(17,12)/CASPT2 G2[21–23] (Complete Active Space Self-Consistent Field/Second-Order Perturbation Theory on a CASSCF wave function) calculations using the standard correlation-consistent cc-pVTZ basis set of Dunning and co-workers[24] $(10s5p2d1f/4s3p2d1f)$. Several basis sets have been previously tested and slight differences in the value of the energy barrier for the transition states of the 2 $^2A'$ and 1 $^2A''$ PES have been found. Table I shows the value of the energy barriers at the CASSCF(17,12)/cc-pVTZ optimized geometry with different basis sets. Differences in the energy barriers are lower than 0.5 kcal mol^{-1}; hence the barrier height is essentially converged with respect to the basis set employed. On the other hand, the CASPT2 perturbation method used is an adequate way[20,25–27] to include the dynamical correlation to the CASSCF wave function. A variational approach such as the MRCI (Multireference Configuration Interaction) method implies to perform excitations over a large number of reference configurations on the CASSCF wave function, as the PES studied involve excited states. However, these calculations are not affordable with the active space (17,12) and the basis set used in the present work.

As our purpose was to study all the PES involved in reaction (2), we have calculated the first two roots in C_s symmetry for the $^2A''$ states at the CASSCF level using equally weighted state average wave functions and CASPT2 calculations were performed on both roots. These calculations have been performed using the MOLCAS 4.1 program.[28] The characterization of all the stationary points at the CASPT2 G2 level and the calculation of their harmonic frequencies have been achieved by fitting different sets of pointwise calculations with the SURVIBTM program[29] of molecular rovibrational analysis.

B. Analytical fit

A NOO′ many-body expansion[30] has been used to obtain an analytical representation of the 1 $^2A''$ PES, which can be written as

$$V(R_1,R_2,R_3)=V_{\mathrm{N}}^{(1)}f(R_1,R_2,R_3)+V_{\mathrm{NO}}^{(2)}(R_1)+V_{\mathrm{OO'}}^{(2)}(R_2)+V_{\mathrm{NO'}}^{(2)}(R_3)+V_{\mathrm{NOO'}}^{(3)}(R_1,R_2,R_3), \tag{3}$$

where $V^{(1)}$, $V^{(2)}$, and $V^{(3)}$ are the one-, two-, and three-body terms, respectively. R_1, R_2, and R_3 are bond displacement coordinates associated with the N–O, O–O′, and N–O′ bond lengths, respectively.

As the O and O′ atoms correlate with its ground electronic state in both reactants and products asymptotes, no one-body terms have been included for them. The N atom, however, changes its electronic state from one asymptote to the other one [ground state, N(^4S), in products and the first excited electronic state, N(^2D), in reactants]. As a consequence, an accurate representation of the PES will be at least two-valued. To obtain a simpler analytical form for the surface we have used a single-valued representation that properly reproduces the two nitrogen atom states in reactants and products asymptotes. This has been achieved by including a one-body term, which consists on the product of the energy of the excited N atom relative to its ground state ($V_{\mathrm{N}}^{(1)}$) and a switching function $f(R_1,R_2,R_3)$, whose value ranges between 0 (products) and 1 (reactants),

$$f(R_1,R_2,R_3)=\frac{1}{2}\left[1-\tanh\left(\frac{\alpha S'}{2}\right)\right], \tag{4}$$

where S' is expressed in terms of displacement coordinates $\{\rho_j=R_j-R_j^0\}$ with respect to a C_{2v}-ONO reference structure (i.e., $R_1^0=R_3^0,R_2^0$), and $\{b_j'\}$ parameters that introduce the correct symmetry of the PES with respect to the O–O′ exchange:

$$S'=\sum_{j=1}^{3} b_j'\rho_j\,. \tag{5}$$

This one-body term ensures the correct asymptotic limits for reaction (2). The parameter α was optimized by means of a trial and error procedure in the global fitting of the PES. This switching function does not assure that a unique value of the energy is obtained when the three atoms are far away from each other. Nevertheless, this uniqueness is not crucial for the study of the interesting PES, because the three separated-atoms region will not be explored under the energy conditions defined in the present study.

Extended-Rydberg potentials have been used to describe the two-body interactions (diatomic energy curves) for NO and O_2:

$$V^{(2)}(R) = -D_e(1 + a_1\rho + a_2\rho^2 + \cdots)e^{-a_1\rho}, \quad (6)$$

where $\rho = (R - R_e)$ is the diatomic internuclear displacement distance, D_e is the equilibrium dissociation energy, and R_e is the equilibrium bond length of the corresponding diatomic molecule. The a_i parameters have been determined by means of a nonlinear least squares fitting of the diatomic *ab initio* points.

The three-body term consists of an *n*-order polynomial $P(S_1,S_2,S_3)$ expressed in terms of symmetry-adapted coordinates (S_1,S_2,S_3) and a range function $T(S_1,S_2,S_3)$, which tends to zero as one of the three atoms separates from the other ones:

$$V^{(3)}_{\mathrm{NOO}'}(R_1,R_2,R_3) = P(S_1,S_2,S_3)T(S_1,S_2,S_3), \quad (7)$$

where

$$P(S_1,S_2,S_3) = \sum_{i,j,k=0}^{0\leq i+j+k\leq n} c_{ijk}S_1^iS_2^jS_3^k, \quad (8)$$

i, j, k being zero or positive integer numbers, and

$$T(S_1,S_2,S_3) = \prod_{i=1}^{3}\left[1 - \tanh\left(\frac{\gamma_i S_i}{2}\right)\right], \quad (9)$$

with

$$S_i = \sum_{j=1}^{3} b_{ij}\rho_j . \quad (10)$$

The number of parameters in the three-body term is reduced, owing to the use of the permutational symmetry of the system. From the sets of linear $\{c_{ijk}\}$ and nonlinear $\{\gamma_i\}$ parameters, those that are associated to odd powers of S_3 (which is antisymmetric with respect to the exchange of the O atoms) are identically zero. The nonzero parameters are determined by a weighted nonlinear least squares procedure using the energies and geometries of the *ab initio* points calculated.

The analytical expression of the $1\,^2A''$ PES has been obtained by means of the same set of programs[31,32] used in previous works of our group[33–39]

C. Kinetics and dynamics methods

The rate constant for reaction (2) has been calculated in a wide range of temperatures using the variational transition state theory (VTST).[40] The calculations have been performed considering the ICVT (improved canonical VTST) method and including the tunnel effect by means of the microcanonical optimized multidimensional (μOMT) correction (ICVT/μOMT method hereafter). These methods have been applied taking into account the analytical PES obtained from the *ab initio* points. The POLYRATE[41] program has been employed to perform these kinetic calculations.

The QCT method[42] as implemented in the TRIQCT[43] program has been used to calculate the rate constant for reaction (2) at several temperatures. Moreover, the mechanism of the reaction through the $1\,^2A''$ PES has also been studied and the NO vibrational distributions at 100 and 300 K have been obtained. The accuracy of the numerical integration of Hamilton's differential equations has been verified by checking the conservation of total energy and total angular momentum for every trajectory and performing back-integrations on sampling trajectories. The integration step size chosen (5×10^{-17} s) was found to achieve these conservation requirements for all the calculated trajectories. The trajectories were started and finished at a distance from the atom to the center of mass of the corresponding diatomic of about 8.0 Å, ensuring that the interaction between fragments was negligible with respect to the available energy. For each temperature, both the relative translational energy (E_T) and the rovibrational levels of the O_2 molecule have been sampled according to a Maxwell–Boltzmann distribution. Approximate final quantized internal distributions [i.e., $P(v')$] were obtained from vibrational radial action variables.

III. RESULTS

A. *Ab initio* study

The reaction between $N(^2D)$ and O_2 on the $1\,^2A''$ PES as in the case of the $2\,^2A'$ PES could take place by means of two different microscopic mechanisms: an abstraction and an insertion mechanism. (See Fig. 1.).

The abstraction mechanism could occur through a very low energetic transition state. The values of the geometry, harmonic frequencies, and energy of this transition state (TS1) at the CASSCF and CASPT2 G2 levels are shown in Table II. The geometry and energy are very similar to the ones of the transition state of the $2\,^2A'$ PES.[20] Both PES show a bent abstraction transition state with large bond distances between the N and O atoms, the distance between both O atoms being very similar to the O_2 equilibrium bond distance (early transition states). Regarding the value of the energy with respect to the reactants, this is very low at the CASPT2 G2 level: 0.25 and 0.08 kcal mol^{-1} for the $1\,^2A''$ and $2\,^2A'$ surfaces, respectively (when including the zero-point energy (ZPE) the following values result: 0.51 and 0.45 kcal mol^{-1}, respectively). Thus, reaction (2) can take place through this mechanism with a very low energetic requirement. The electronic configuration of the wave function along the abstraction mechanism of the PES is clearly multiconfigurational, that is to say, there are several electronic configurations that contribute significantly to the CASSCF wave function.

The insertion mechanism is more complicated due to the presence of intersections between PES along the minimum energy path (MEP), as two PES of the same symmetry (spin and space), in this case the $1\,^2A''$ and $2\,^2A''$ surfaces, can cross in contrast to what happens for diatomic molecules.[44,45] In fact, the noncrossing rule only applies to diatomic molecules, whereas, in general, an intersection seam of dimension M-2 can exist, where *M* is the number of independent internal coordinates for the molecular symmetry considered. Therefore, for the NOO system in C_s symmetry one has $M = 3$ independent internal coordinates and, consequently, it is

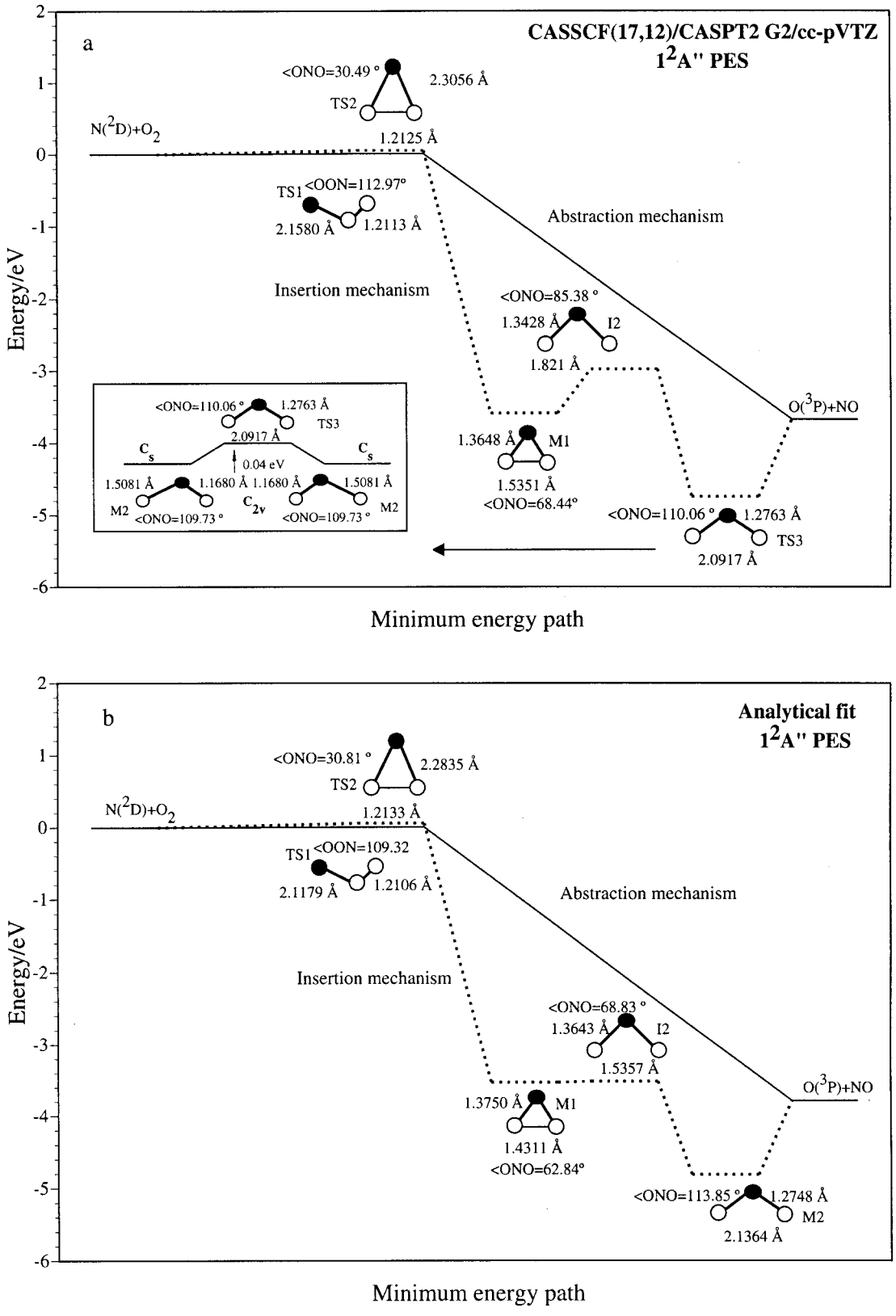

FIG. 1. Energy diagram of the stationary points located in the minimum energy path of the $1\,^2A''$ PES: (a) *ab initio* level; (b) analytical PES. In the analytical PES the intersection I2 really corresponds to a saddle point. Energies are given in eV relative to reactants $N(^2D)+O_2$.

feasible to have a one-dimensional (i.e., a line) intersection seam. Moreover, in case the surfaces belong to different irreducible representations in a restricted space of higher symmetry (in this case the $1\,^2A''$ and $2\,^2A''$ PES presents $^2A_2$ and $^2B_1$ symmetries in C_{2v}) the intersection seam entirely lies in the restricted coordinate space. In this work, we have located the minimum energy point along the line of intersection between the two lowest $^2A''$ surfaces. The dimensionality rules,

TABLE II. Properties of the stationary points of the $1\,^2A''$ PES.

	R_{NO}/Å	R_{OO}/Å	<NOO/°	ω_i/cm^{-1}	E/kcal mol^{-1} [a]
Reactants $[N(^2D)+O_2]$					
CASSCF		1.2177		1541.74	0
CASPT2 G2		1.2091		1586.18	0
Analytical fit		1.2075		1610.1	0
Products $[O(^3P)+NO]$					
CASSCF	1.1587			1895.63	−102.33
CASPT2 G2	1.1543			1904.45	−85.02
Analytical fit	1.1508			1887.6	−87.28
Transition state of the abstraction mechanism (TS1) (C_s)					
CASSCF	1.9286	1.2318	108.20	441.07i(ω_a), 106.26(ω_b), 1376.44(ω_s)	6.83 (6.74)
CASPT2 G2	2.1580	1.2113	112.97	164i(ω_a), 235(ω_b), 1534(ω_s)	0.25 (0.51)
Analytical fit	2.118	1.211	109.3	174i(ω_a), 131(ω_b), 1543(ω_s)	0.21 (0.30)
	$R_{NO'}$/Å	$R_{NO''}$/Å	<ONO/°	ω_i/cm^{-1}	E/kcal mol^{-1}[a]
Transition state $^2A_2$ *of the insertion mechanism* (TS2) (C_{2v})[b]					
CASSCF	2.2149	2.2149	32.08	138.88(ω_a), 1490.22(ω_b), 320.66i(ω_s)	5.29 (5.42)
CASPT2 G2	2.3056	2.3056	30.49	180(ω_a), 1629(ω_b), 217i(ω_s)	1.25 (1.57)
Analytical fit	2.284	2.284	30.8	158i(ω_a), 1411(ω_b), 229i(ω_s)	1.43 (1.15)
Minimum $^2B_1$*-ring form of* NO_2 (M1) (C_{2v})					
CASSCF	1.3809	1.3809	67.78	668.59(ω_a), 740.84(ω_b), 1217.93(ω_s)	−75.63 (−74.07)
CASPT2 G2	1.3648	1.3648	68.44	613(ω_a), 722(ω_b), 1239(ω_s)	−82.79 (−81.38)
Analytical fit	1.3750	1.3750	62.8	800(ω_a), 506(ω_b), 1269(ω_s)	−81.40 (−80.02)
Peaked intersection in the insertion path (I2) (C_{2v})					
CASSCF	1.349	1.349	84.29		−59.41
CASPT2 G2	1.343	1.343	85.38		−68.66
Analytical fit	1.363	1.363	68.8		−81.08
Transition state $^2A_2$ (TS3) (C_{2v})					
CASSCF	1.2857	1.2857	109.92	721.26i(ω_a), 757.68(ω_b), 1302.99(ω_s)	−107.61 (−105.84)
CASPT2 G2	1.2763	1.2763	110.06	432i(ω_a), 777(ω_b), 1300(ω_s)	−109.38 (−108.68)
Analytical fit[c]	1.2748	1.2748	113.8	826(ω_a), 588(ω_b), 1082(ω_s)	−110.9 (−109.63)
Distorted minimum (M2) (C_s)[d]					
CASSCF	1.5834	1.1619	109.58	339.24($\omega_{NO'}$), 703.26(ω_b), 1733.81($\omega_{NO''}$)	−111.25 (−109.48)
CASPT2 G2	1.5081	1.1680	109.73	310($\omega_{NO'}$), 768(ω_b), 1735($\omega_{NO''}$)	−110.29 (−108.54)

[a]Energy referred to reactants. Between parentheses is given $E+$ZPE, where ZPE is the zero-point energy.
[b]In the analytical fit this stationary point is a second-order saddle point.
[c]This point is a minimum in the analytical PES (see the text).
[d]The distorted minimum is not reproduced in the analytical PES.

however, do not guarantee the surfaces to cross, the existence of an avoided intersection between them being possible.

The lowest-energy point on the first intersection seam (II) between the surfaces of $^2A_2$ and $^2B_1$ symmetry has been located at the beginning of the MEP and after an insertion transition state (TS2) of only 1.25 kcal mol^{-1} above reactants (1.57 kcal mol^{-1} including ZPE) that belongs to the $1\,^2A_2$ PES. The topology of this intersection is sloped, that is to say, both surfaces decrease monotonically and touch each other along the slope. Thus, we can only appreciate a slightly change in the slope of the adiabatic PES near the intersection. In this case and in the excited PES we have localized a NO_2 minimum. For this reason, the shape of this intersection in the $2\,^2A''$ PES is a little different from what has to be expected for a standard sloped intersection. Table II shows the geometry and energy of this crossing at the CASSCF(17,12) level. Figure 2 shows the shape of the $1\,^2A''$ and $2\,^2A''$ PES near the crossing point using Jacobi coordinates (a cross marks the location of the intersection point of lowest energy along the seam). Figure 3 shows the bending plot (variation of energy in both surfaces with the ONO angle) for the same intersection.

After the intersection, the electronic configuration of the adiabatic PES changes from $^2A_2$ into $^2B_1$ symmetry. In this part of the PES and for a small ONO angle of about 69°, we have found a minimum (M1). The existence of this minimum called the ''ring form'' of NO_2, has been noted before.[18,46] However, to the best of our knowledge, this is the first time that a complete description of its properties (geometry, harmonic frequencies, and energy) is reported. The wave function in this part of the PES has a clear monoconfigurational character, as only one electronic configuration contributes significantly to the wave function.

Another intersection (I2) (Table III and Figs. 2 and 3) between $1\,^2A''$ and $2\,^2A''$ PES is found after the $^2B_1$ minimum. In this case the topology of the intersection is peaked (it has the form of a tilted double cone, where the lower surface decreases in all directions from the intersection point and the upper surface increases in all directions from the same point) and it is located 12.72 kcal mol^{-1} above the $^2B_1$ minimum. In this point, the electronic configuration of the adiabatic PES changes again from $^2B_1$ into $^2A_2$ symmetry.

At the end of the insertion pathway we have found another stationary point which frequencies corresponding to the normal mode of bending and symmetric stretching are real

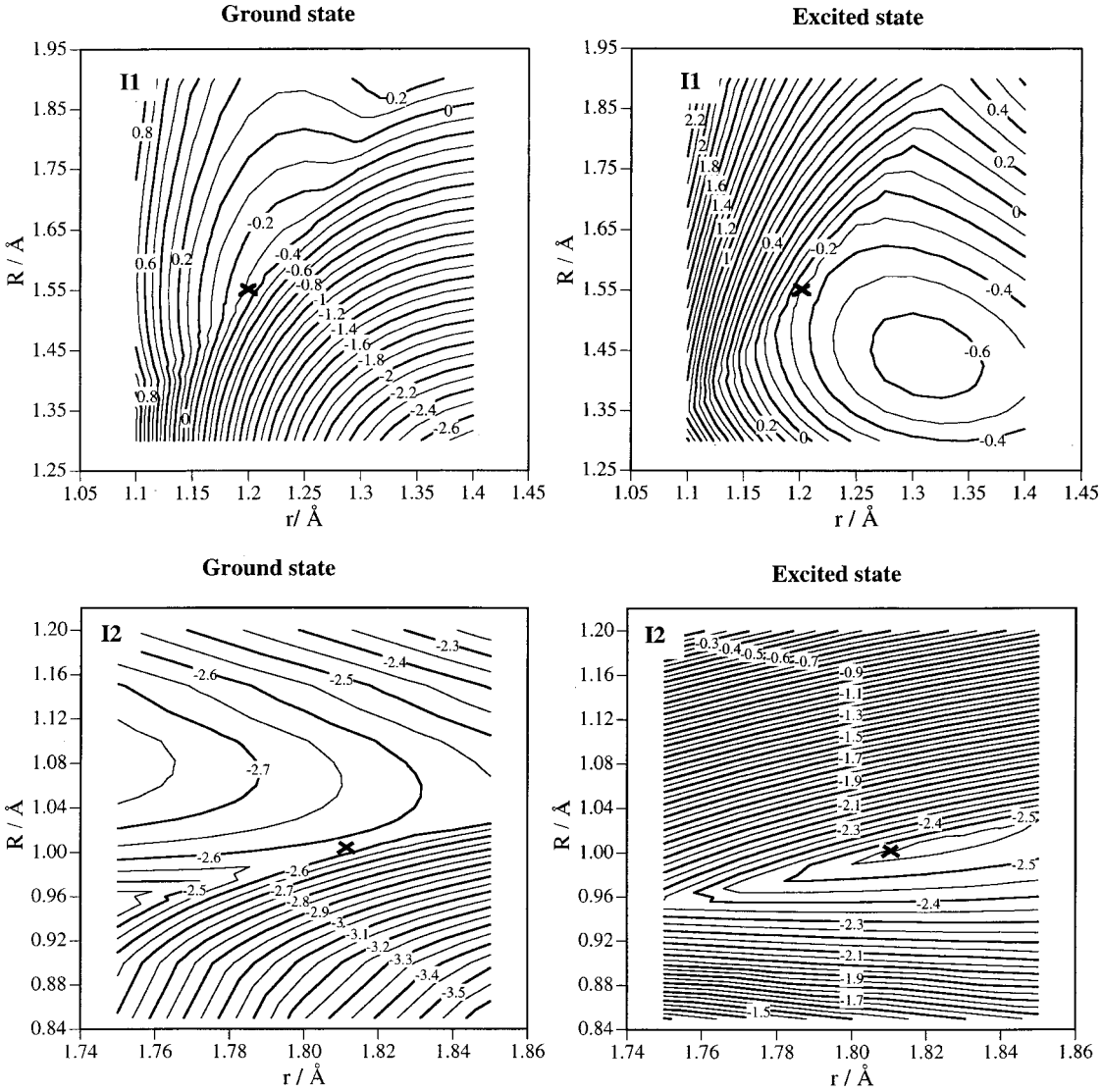

FIG. 2. Contour diagrams of the $1\,^2A''$ and $2\,^2A''$ PES for C_s symmetry tending to C_{2v} symmetry, using Jacobi coordinates [R and r correspond to the $N(^2D)-O_2$ and O_2 distances, respectively]. The location of the I1 and I2 intersections is evident from these plots, and the point of lowest energy along the seam of the intersections is indicated by a cross. Energy in eV referred to reactants $N(^2D)+O_2$.

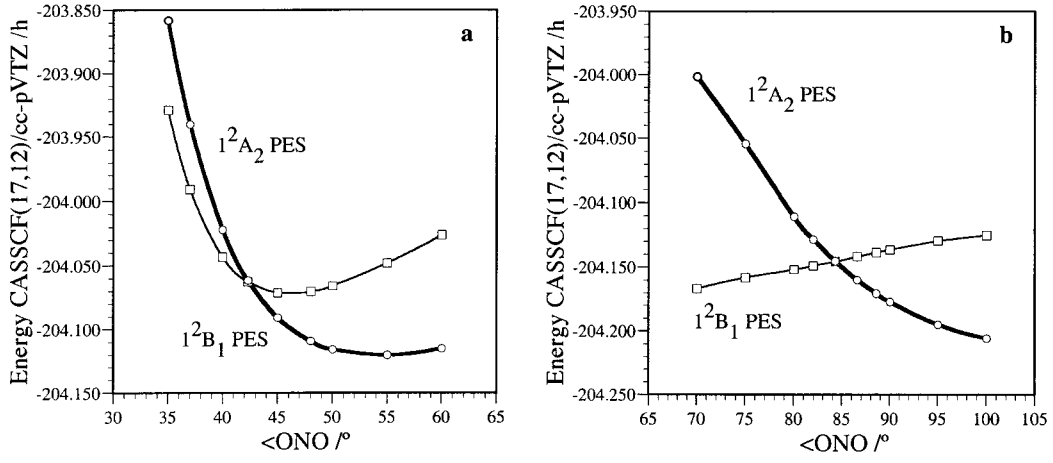

FIG. 3. The C_{2v} ONO bending absolute energy curves considering the NO distance of the lowest-energy point along the intersection seam of I1 (a) and I2 (b).

TABLE III. Location and energetics of the CASSCF(17,12)/cc-pVTZ lowest energy point of the $1\,^2A''-2\,^2A''$ intersection seams.

	I1	I2
R_{NO}/Å	1.6621	1.3487
R_{OO}/Å	1.2000	1.8100
<ONO/°	42.32	84.29
ΔE/kcal.mol^{-1}[a]	0.57	0.16
$1\,^2A''C_i$(CSFs)[b]	−0.903 76, 0	0.901 47, 0
$2\,^2A''C_i$(CSFs)[b]	0, 0.894 86	0, 0.887 86

[a]Energy difference between the ground and the first excited $^2A''$ surfaces at both geometries.

[b]Coefficients (C_1, C_2) of the two most important CSFs (configuration state functions) in the CASSCF wave function, CSFs ($9a'$, $3a''$) for CASSCF(17,12). Occupation numbers are the following (222222000 212) (222222000 221) for I1 and (222222200 210) (222222000 221) for I2.

but the asymmetric stretching presents an imaginary frequency. Therefore, this C_{2v} structure must be a transition state (TS3) and connect two minima. We have also found the properties of these two minima (M2). In fact, they correspond to equivalent C_s structures and the C_{2v}-transition state of $^2A_2$ symmetry allows the interconversion between them. This excited state of NO_2 has also been described in previous theoretical and experimental works.[47–50] However, while the experimental structure reported has C_{2v} symmetry, several theoretical works have predicted the existence of distorted C_s equivalent structures for this minimum. According to Ref. 46, this excited state of NO_2 with $^2A_2$ symmetry may suffer from a pseudo-Jahn–Teller distortion due to the interaction with the higher lying $^2B_1$ state via the asymmetric stretching vibration. On the other hand, the C_s minimum is located only 0.91 kcal mol^{-1} below the C_{2v}-transition state at the CASPT2 G2 level, and if we take into account the zero-point energy (ZPE), the C_s structure is 0.14 kcal mol^{-1} more energetic than the C_{2v} structure. Therefore, we can conclude that the dynamical symmetry of this excited state of the NO_2 is C_{2v} and that the N–O bond length inferred from experiment would roughly correspond to an average of the two distances in the C_s structure. As in the case of M1, the wave function in this part of the PES also has a monoconfigurational character.

Finally, this C_s structure correlates with the products of reaction (2) on the $1\,^2A''$ PES without the presence of any saddle point. The properties (geometry, frequencies, and energy) of all stationary points implied in the insertion mechanism through the $1\,^2A''$ PES can be found in Table II. In Table IV we present a comparison between the properties of the excited states of NO_2 found in this work and the ones reported in recent studies.

As a conclusion, either the abstraction mechanism or the insertion mechanism could take place through the $1\,^2A''$ PES. However, the energetic requirement of the abstraction mechanism (around 0.5 kcal mol^{-1}) is lower than the one for the insertion mechanism. Moreover, in the insertion mechanism we have found the presence of two excited states of the NO_2 minimum and of several intersections between the $1\,^2A''$ and the $2\,^2A''$ PES that make possible electronically nonadiabatic transitions between them.

B. Analytical fit

The fitting of the potential energy curves of O_2 and NO has been carried out using the calculated diatomic *ab initio* points (20 and 25 points for O_2 and NO, respectively), and an extended Rydberg potential up to third order for O_2 and fifth order for NO has been employed. The values of the equilibrium dissociation energy (D_e) and bond distance (R_e) used in the fitting procedure are the experimental ones because in this way we can exactly reproduce the energetics of reaction (2). The root-mean-square deviation (RMSD) for the diatomic curves of O_2 and NO are 0.39 and 0.53 kcal mol^{-1}, respectively. The optimal extended Rydberg parameters of each diatomic molecule are given in Table V and the spectroscopic constants derived from them are given in Table VI.

The value of the one-body term is taken as the experimental energetic requirement for the process $N(^4S) \rightarrow N(^2D)$[3]. This one-body term ensures a single-valued rep-

TABLE IV. Properties of the excited states of NO_2.

	$R_{NO'}$/Å	$R_{NO''}$/Å	<ONO/°	ω_i/cm^{-1}	E/kcal mol^{-1} [a]
Minimum $^2B_1$-ring form of NO_2 (M1) (C_{2v})					
CI (Ref. 46)	1.40	1.40	75		69.72
CASSCF MP2 (Ref. 18)	1.37	1.37	69		79.33
This work CASSCF	1.3809	1.3809	67.78	668.59(ω_a), 740.84(ω_b), 1217.93(ω_s)	75.61
This work CASPT2	1.3648	1.3648	68.44	613(ω_a), 722(ω_b), 1239(ω_s)	80.25
Distorted minimum (M2) (C_s)					
MCSCF (Ref. 47)	1.27	1.27	110	798(ω_b), 1360(ω_s)	42.43
CCSD (Ref. 48)	1.303	1.274	109.4		44.57
QRHF CCSD (T) (Ref. 49)	1.513	1.183	109.5		
Expt. (Ref. 50)	1.339±0.01	1.339±0.01	108.4±1.0	250(ω_a), 750(ω_b), 1010(ω_s)	46.40
This work CASSCF	1.5834	1.1619	109.58	339.24($\omega_{NO'}$), 703.26(ω_b), 1733.81($\omega_{NO''}$)	39.98
This work CASPT2	1.5081	1.1680	109.73	310($\omega_{NO'}$), 768(ω_b), 1735($\omega_{NO''}$)	52.75

[a]Energy referred to the ground state of $NO_2(X\,^2A_1)$.

TABLE V. Optimal parameters of the $1\,^2A''$ analytical PES.

One-body parameters							
$V_N^{(1)}$/eV		α_1/Å^{-1}		b_1'	b_2'		b_3'
2.3835		1.543 60		−1	3		−1
Two-body parameters							
Species	D_e/eV	R_e/Å	a_1/Å^{-1}	a_2/Å^{-2}	a_3/Å^{-3}	a_4/Å^{-4}	a_5/Å^{-5}
O–O	5.2132	1.2075	5.458 19	7.581 88	5.115 49		
N–O	6.6144	1.1507	3.848 32	0.007 46	0.909 85	−6.264 02	4.291 64
Three-body parameters							
c_{000}	0.722 526	c_{102}	−3.878 49	c_{022}	−19.2622	c_{104} 6.463 68	c_{240} 42.1305
c_{100}	−0.065 327 7	c_{030}	29.394 09	c_{004}	2.330 65	c_{050} −24.6928	c_{222} −7.407 19
c_{010}	−2.310 61	c_{012}	−4.931 91	c_{500}	0.300 729	c_{032} −11.3022	c_{204} −0.229 995
c_{200}	3.305 33	c_{400}	0.293 570	c_{410}	−1.324 29	c_{014} 3.935 40	c_{150} −22.2739
c_{110}	−0.782 257	c_{310}	−0.209 408	c_{320}	−7.101 57	c_{600} 0.287 496	c_{132} −22.0082
c_{020}	6.445 784	c_{220}	−7.675 03	c_{302}	2.513 39	c_{510} 0.548 994	c_{114} 4.658 86
c_{002}	2.305 52	c_{202}	−2.495 03	c_{230}	−9.718 98	c_{420} −3.260 64	c_{060} 7.175 38
c_{300}	0.400 585	c_{130}	39.9638	c_{212}	−8.420 32	c_{402} 0.595 284	c_{042} 7.884 13
c_{210}	5.180 22	c_{112}	−10.8210	c_{140}	42.7277	c_{330} −20.1527	c_{024} 4.494 11
c_{120}	1.159 79	c_{040}	6.506 81	c_{122}	−11.1881	c_{312} 14.1041	c_{006} −1.684 80
$R_1^0=R_3^0$/Å		R_2^0/Å		γ_1/Å^{-1}		γ_2/Å^{-1}	γ_3/Å^{-1}
2.054 70		1.539 00		3.040 92		2.763 46	0.0
				b_{ij} $i,j=1,2,3$			
				$\sqrt{(1/2)}$ 0.0 $\sqrt{(1/2)}$			
				0.0 1.0 0.0			
				$\sqrt{(1/2)}$ 0.0 $-\sqrt{(1/2)}$			

[a]Units for coefficients are eV Å$^{-(i+j+k)}$.

resentation of the PES, being the electronic atomic state of the nitrogen atom reproduced correctly in reactants $[N(^2D)]$ and in products $[(N^4S)]$.

As regards the three-body term, we have used as a reference structure an average of the geometries of TS1, TS2, TS3, and M1.

The *ab initio* data employed to determine the three-body parameters are the following: (a) energy and geometry of the *ab initio* stationary points; (b) 424 *ab initio* points for the abstraction mechanism (C_s symmetry, NOO arrangement) and 456 *ab initio* points for the insertion mechanism (C_{2v} symmetry, ONO arrangement). Although most of the *ab initio* points are concentrated near the stationary points, the asymptotes have also been widely explored to provide a good description of the PES along the minimum energy path; (c) about 210 points interpolated between the *ab initio* points by means of bicubic splines, that allows us to eliminate spurious structures in the entrance and exit channels. As in the fitting of the $2\,^2A'$ PES, the points have been properly scaled by shifting the value of their energy to reproduce the energetics of reaction (2) and the dissociation energy of the diatomic molecules. The whole set of points was fitted to a sixth-order polynomial. In Table V are shown the optimal parameters of the $1\,^2A''$ analytical PES. There are 87 parameters but, as 35 of them are equal to zero by symmetry, this leads to 52 parameters to be optimized, 50 of which are linear (the polynomial coefficients) and 2 are nonlinear (γ_1 and γ_2).

In general, there is a good agreement between the *ab initio* properties of the stationary points and those resulting from the fitting (Table II and Fig. 1). The RMSD of the points located in the abstraction and insertion parts of the PES is equal to 2.26 and 2.75 kcal mol^{-1}, respectively, while the RMSD of the PES is 2.47 kcal mol^{-1}.

The description of the MEP along the abstraction mechanism is very good, as the properties of the analytical transition state (TS1) are very close to the properties of the *ab initio* one. However, it has not been possible to reproduce properly all the stationary points involved in the insertion mechanism. The energetics and geometry of the transition

TABLE VI. Spectroscopic constants of the diatomic molecules.

Species	D_e/eV[a]	R_e/Å[a]	ω_e/cm^{-1}	$\omega_e x_e$/cm^{-1}	B_e/cm^{-1}	α_e/cm^{-1}
O_2						
Analytical fit	5.2132	1.2075	1610.1	12.554	1.445 30	0.0152
Expt. (Ref. 51)	5.2132	1.2075	1580.2	11.981	1.445 63	0.0159
NO						
Analytical fit	6.6144	1.1508	1887.6	13.569	1.704 47	0.0193
Expt. (Ref. 51)	6.6144	1.1508	1904.2	14.100	1.671 95	0.0171

[a]The value of D_e and R_e included in the fit are the experimental ones. The *ab initio* [CASSCF (17,12)/CASPT2 G2/cc-pVTZ] values for D_e and R_e are 5.3362 eV and 1.2091 Å for O_2, and 6.4912 eV and 1.1543 Å for NO, respectively.

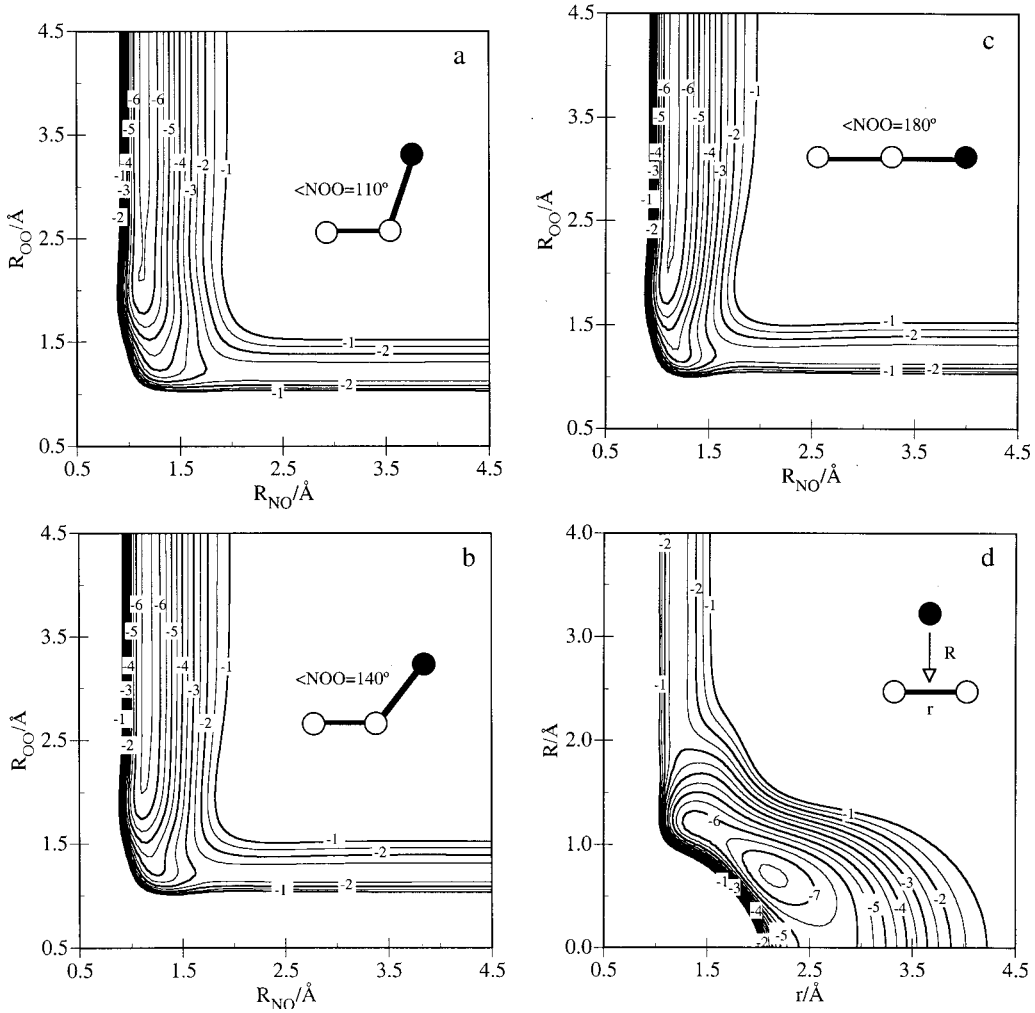

FIG. 4. Contour diagrams of the $1\,^2A''$ analytical PES at different <NOO angles: (a) 110°, (b) 140°, (c) 180°, and (d) NO_2 (C_{2v} arrangement described using Jacobi coordinates). The contours are depicted in increments of 0.5 eV and the zero of energy is taken at $N(^4S)+O(^3P)+O(^3P)$.

state at the entrance channel is well reproduced, however, it has not been possible to obtain the correct harmonic frequencies. While at the *ab initio* level this point presents only one imaginary frequency in the analytical PES, it corresponds to a second-order transition state (two imaginary frequencies). As refers the minimum $^2B_1$ (M1), it has also been possible to reproduce quite well its geometry, energy, and harmonic frequencies. Unfortunately, as refers the intersection (I2), the $^2A_2$ transition state (TS3) and the distorted minimum (M2), they have not been correctly reproduced. While the intersection is situated 12.72 kcal mol^{-1} above the $^2B_1$ minimum at the CASPT2 G2 level, it is located only 0.32 kcal mol^{-1} above this minimum in the analytical fit. Several attempts to improve the description of this part of the PES have been carried out. However, it has not been possible to attain a better fit of the *ab initio* data around the intersection I2 by means of the analytical function used in this work. For the purpose of the present work, it is enough to consider this kind of representation, although for studies including nonadiabatic interactions a multivalued analytical representation would be required. Nevertheless, from the present approach it is expected that the reaction dynamics will not be strongly affected by the not so well-described intersection I2. In fact, the high exoergicity of the reaction and the minimum M2 are expected to be much more important to define the properties of products. As refers the C_{2v} structure of symmetry $^2A_2$, at an *ab initio* level it corresponds with a saddle point and a minimum with distorted symmetry is located 0.91 kcal mol^{-1} below. In the analytical PES, it has not been possible to reproduce these structures and in this part of the PES there is only a stationary point of C_{2v} symmetry whose geometry and energy are quite similar to the ones of the transition state (TS3). Nevertheless, in the analytical fit this point is a minimum, while at the *ab initio* level it corresponds to a transition state.

The contour diagrams at several NOO angles (110°, 140°, and 180°) and the contour diagram for the ONO-C_{2v} arrangement are shown in Fig. 4.

C. Rate constants

The thermal rate constant through the $1\,^2A''$ PES of reaction (2) has been calculated by means of the QCT method at 100, 200, 300, 400, 500, 1000, and 2000 K. Furthermore, we have also considered the VTST method to calculate the rate constant. Unfortunately, in our analytical PES TS2 is not

TABLE VII. Rate constants of the 1 $^2A''$ analytical PES at different levels of theory.[a]

T/K	ICVT[b]	ICVT/μOMT[b]	QCT[c]
100	6.72×10^{-13}	8.38×10^{-13}	$(7.70\pm0.4)\times10^{-13}$
200	2.18×10^{-12}	2.31×10^{-12}	$(2.47\pm0.08)\times10^{-12}$
300	4.02×10^{-12}	4.11×10^{-12}	$(3.81\pm0.11)\times10^{-12}$
400	5.97×10^{-12}	6.06×10^{-12}	$(5.37\pm0.12)\times10^{-12}$
500	8.03×10^{-12}	8.11×10^{-12}	$(6.77\pm0.13)\times10^{-12}$
1000	1.83×10^{-11}	1.84×10^{-11}	$(1.28\pm0.02)\times10^{-11}$
2000	3.86×10^{-11}	3.86×10^{-11}	$(2.11\pm0.03)\times10^{-11}$

[a]Units are cm^3 $molecule^{-1}$ s^{-1}.
[b]Calculated taking into account the ICVT and ICVT/μOMT rate constant of TS1 in the analytical PES and the increase in reactivity due to TS2 at the TST and TST/Wigner level (see the text).
[c]Statistical errors correspond to one standard deviation.

satisfactorily described in what regards to the frequencies, so we have only managed to apply the ICVT method (with the μOMT tunneling correction) to TS1. However, reactivity can also take place by means of an insertion mechanism through TS2 and the rate constant for the 1 $^2A''$ PES is given by the sum of the rate constants obtained through TS1 and TS2. To take into account the influence of TS2 in the ICVT and ICVT/μOMT rate constant, we have carried out both a TST and a TST/Wigner study of this rate constant using the *ab initio* structures of both the abstraction (TS1) and the insertion (TS2) transition states. In this way, we have calculated at the TST and TST/Wigner levels the increase in percentage in the value of the global rate constant due to the insertion mechanism (TS2) and have applied this same increase to the value of the ICVT and ICVT/μOMT rate constant calculated by means of the analytical PES, where only TS1 is satisfactorily described. Taking into account this approximation the values obtained by VTST and QCT methods are, in general, quite close to each other. The largest difference between both methods occurs at 2000 K, where we can appreciate a discrepancy of about 17% between the QCT and ICVT values. Regarding the tunnel effect, it is only important at the lowest temperature (100 K), where reactivity increases about 20% because of this effect. The importance of tunneling, however, quickly decreases as temperature increases because heavy atoms are involved. Table VII and Fig. 5 shows the values of the rate constant for the 1 $^2A''$ PES at different levels of theory. There is some curvature in the Arrhenius' representation of the rate constants at both the VTST (with and without tunneling) and QCT levels. This fact shows that the rate constants present a non-Arrhenian behavior, that is to say, both the pre-exponential factor and the activation energy depend on the temperature. This feature is expected when a wide range of temperatures is explored.

The rate constant for reaction (2) can be expressed as

$$k(2)=k(2\,^2A')+k(1\,^2A''), \tag{11}$$

where the ratio between the electronic partition functions of the corresponding saddle point and those of reactants has been taken as

$$\frac{Z_{\mathrm{el,TS}}}{Z_{\mathrm{el,N}(^2D)}\cdot Z_{\mathrm{el,O_2}}}=\frac{2}{[6+4\exp(-12.536/T)]\cdot 3}, \tag{12}$$

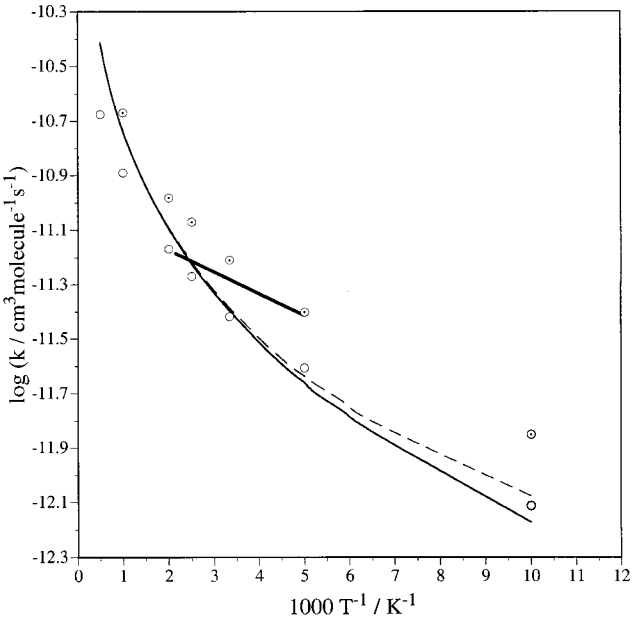

FIG. 5. Arrhenius' plot of the calculated rate constant for the 1 $^2A''$ analytical PES: ICVT (—), ICVT/μOMT (– – –), and QCT (○) values. Arrhenius' plot of the rate constants of reaction (2): QCT values taking into account the contributions of the 1 $^2A''$ and 2 $^2A'$ PES (⊙) and recommended experimental data[17] (——). In the case of the experimental results the two reactive channels and the physical electronic quenching are included. That is to say, they correspond to the global rate constant for the deactivation of N(^2D) (see the text). The QCT error bars correspond approximately to the size of the symbol.

where we have taken into account the electronic states that adiabatically correlate reactants and products and have neglected electronically nonadiabatic effects. The value of 12.536 K of Eq. (12) corresponds to the energy of the excited spin–orbit (SO) state of the N(^2D) atom ($^2D_{3/2}$) relative to the ground SO state ($^2D_{5/2}$), 8.713 cm^{-1}, divided by the molar gas constant (R).

Even though reaction (2) has six PES that adiabatically correlate reactants and products, at temperatures below 1000 K only the 2 $^2A'$ and 1 $^2A''$ PES have low enough energy barriers to be involved in reactivity. Thus, because of this, these PES are the only ones that appear in Eq. (11). As we have also studied in a previous paper[20] the 2 $^2A'$ PES, we have been able to calculate the rate constant of reaction (2) at different temperatures at both the VTST and QCT levels. The values of these rate constants and a comparison with the experimental[17] ones can be found in Table VIII and Fig. 5. The agreement between the experimental and theoretical values is very good at temperatures below 300 K and it becomes slightly worse at temperatures between 300 and 400 K. However, in both cases the theoretical results are within the experimental estimated error margins [at room temperature,[2–14] it may be found that $k=(5.2\pm1.1)\times10^{-12}$ cm^3 $molecule^{-1}$ s^{-1}].

D. Dynamical properties

To perform a rigorous study of the dynamics of the N(^2D)+O_2 system, the possibility of nonadiabatic transitions between the different PES involved should be taken

TABLE VIII. Rate constants of reaction (2)[a]

T/K	ICVT[b]	QCT[c]	$k(T)$ global[d] Experimental[e]
100	1.26×10^{-12}	1.41×10^{-12}	
200	3.68×10^{-12}	3.96×10^{-12}	3.85×10^{-12}
300	6.36×10^{-12}	6.16×10^{-12}	5.24×10^{-12}
400	9.13×10^{-12}	8.50×10^{-12}	6.11×10^{-12}
500	1.20×10^{-11}	1.04×10^{-11}	
1000	2.62×10^{-11}	2.14×10^{-11}	

[a]Units are cm^3 molecule^{-1} s^{-1}.
[b]Taking into account the ICVT results of our previous paper (Ref. 20) (see the text).
[c]Taking into account the QCT results of our previous paper (Ref. 20) (see the text).
[d]Including both reactive channels [reactions (1) and (2)] and the physical electronic quenching of N(^2D).
[e]Reference 17.

into account. However, as a first approach, we will study some dynamics properties of this system by means of the quasiclassical trajectory method neglecting nonadiabatic effects.

The QCT vibrational distributions of NO at 100 K on the $1\,^2A''$ PES have been calculated and after taking into account the $2\,^2A'$ results reported in Ref. 20 have been compared with the experimental results at 100 K.[19] Figure 6(a) shows the vibrational distribution of products obtained here from the $1\,^2A''$ PES and previously[20] from the $2\,^2A'$ PES. There are important differences between the vibrational populations obtained in both PES. While the $2\,^2A'$ PES leads to a clearly inverted distribution peaked at $v'=9$, the $1\,^2A''$ PES leads to a less excited vibrational distribution peaked at $v'=6$, being more similar to the experimental values.

TABLE IX. NO vibrational distributions from reaction (2) at 100 K.[a]

v'	QCT	Experimental[b]
0	0.0364±0.0027	0.0000
1	0.0347±0.0026	0.0000
2	0.0397±0.0029	0.0720±0.0356
3	0.0415±0.0030	0.0544±0.0293
4	0.0442±0.0031	0.1186±0.0175
5	0.0637±0.0042	0.1749±0.0265
6	0.0982±0.0063	0.1701±0.0265
7	0.1461±0.0092	0.1848±0.0287
8	0.1399±0.0090	0.1122±0.0258
9	0.1468±0.0094	0.0720±0.0223
10	0.1440±0.0093	0.0313±0.0062
11	0.0531±0.0041	0.0098±0.0082
12	0.0069±0.0009	0.0000
13	0.0026±0.0005	0.0000
14	0.0022±0.0005	0.0000
15	0.0011±0.0003	0.0000
16	0.0001±0.0001	0.0000
17	0.0002±0.0001	0.0000
18	0.0002±0.0001	0.0000

[a]Populations are normalized to unity.
[b]Reference 19.

The vibrational distributions of products for reaction (2) at 100 K have also been calculated, taking into account the values obtained from both PES and compared with the experimental values available at this temperature[19] and with the theoretical results of Ref. 18 at 500 K [Table IX and Fig. 6(b)]. The global vibrational distributions have been obtained after proper averaging of the populations obtained from the $2\,^2A'$ and $1\,^2A''$ PES [both surfaces have the same weight, as indicated in the rate constant calculation, Eq. (12)].

The agreement between the theoretical and the experi-

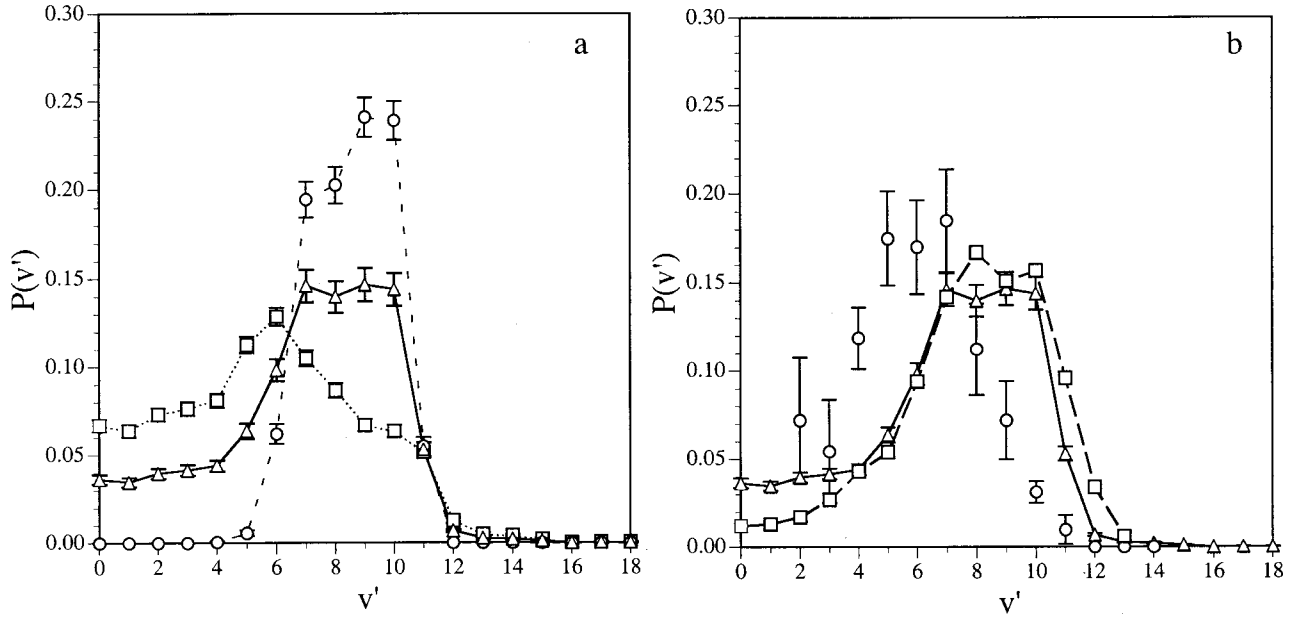

FIG. 6. Vibrational distributions of NO from reaction (2) at 100 K: (a) QCT results on the $1\,^2A''$ analytical PES (□), QCT results on the $2\,^2A'$ PES (Ref. 20) (○), and global results (△); (b) QCT global results for reaction (2) (△), QCT global results for reaction (2) (□) (Ref. 18, 500 K), and experimental data (Ref. 19) (○).

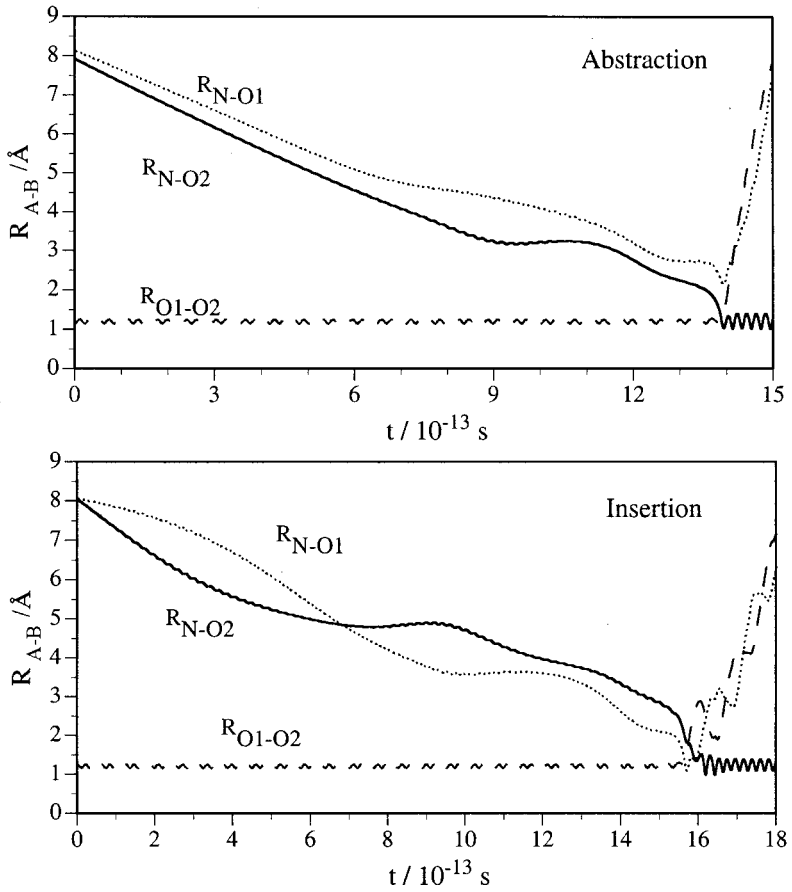

FIG. 7. Representative reactive trajectories corresponding to the abstraction and insertion mechanisms.

mental vibrational distributions for the reaction at 100 K is only qualitative. The experimental populations peak near $v'=7$, whereas according to our QCT results, the $v'=7$, 8, 9, 10 vibrational levels are equally populated being $\langle v' \rangle = 5.64$. The QCT results show that the vibrational levels corresponding to $v'=0$, 1 are slightly populated. Experimentally the population of these levels is not reported because of the difficulty in extracting these populations from the measured spectra. The difference between experimental and theoretical results could be due to the above-mentioned limitations of the calculations, but also to the existence of some vibrational relaxation in the experimental measurements.

There is a good agreement between both the present and previous[18] QCT results, although higher-energy barriers for the transition states were obtained in Ref. 18. This fact suggests that the features of the PES after the barrier (particularly, the large exoergicity of the reaction) essentially controls the populations of the NO internal states. However, the vibrational results of Ref. 18 were calculated at 500 K, due to the energy barrier of the PES. In contrast, our vibrational distributions are calculated at the experimental temperature of 100 K.

The vibrational distributions obtained in this work clearly improve the ones of our previous paper,[20] where only the $2\,^2A'$ PES was considered. However, the agreement between theoretical and experimental work is yet only qualitative. Further work is necessary to clarify the origin of this discrepancy.

The differences that appear in the vibrational distributions of NO derived from both PES are due to the existence of different microscopic mechanisms of reaction. While under the reaction conditions explored, reactivity on the $2\,^2A'$ PES takes place only by an abstraction mechanism, the $1\,^2A''$ PES could present two different modes of reaction because of the very-low- and low-energy barriers of the saddle points that allow either the insertion or the abstraction mechanisms, respectively. Reactive trajectories that evolve through the abstraction mechanism are the ones in which there is always an oxygen atom that along the whole trajectory remains at a large distance ($\geqslant$2.0 Å) of the nitrogen atom and the value of the energy never becomes lower than the products energy. On the other hand, for the reactive trajectories corresponding to the insertion mechanism, there is a point along the evolution to products where the distances of the attacking nitrogen atom to both oxygen atoms have the same value (C_{2v} geometry). At this point the system is located not far from the NO_2 minimum and the value of the energy of the system at this point is lower than the products energy (Fig. 7).

The properties of the products of reaction are different for both mechanisms. Trajectories that have taken place through the abstraction mechanism present excited vibrational distributions peaked at $v'=6$, as expected for a reaction with high exothermicity, while in the case of the insertion mechanism the vibrational distribution is less excited and peaked at $v'=2$. One of the reasons of this fact could be that the insertion mechanism allows trajectories to pass

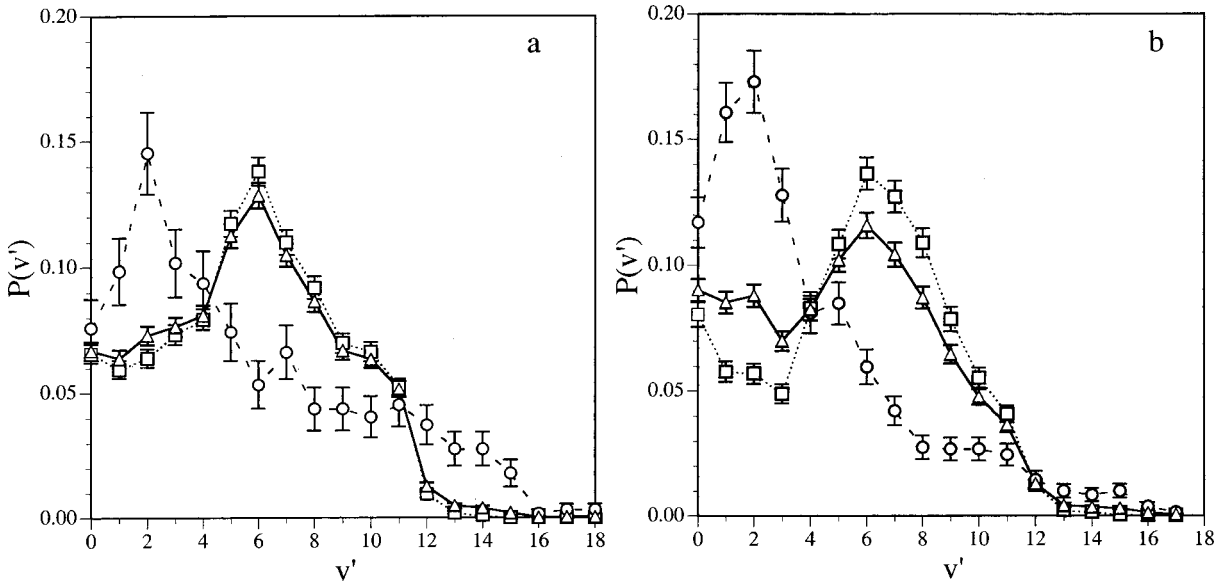

FIG. 8. Vibrational distributions of NO from reaction (2) at 100 K (a) and 300 K (b) on the $1\,^2A''$ analytical PES: abstraction mechanism (□), insertion mechanism (○), and global (△).

through the minimum of the PES and in this way they could distribute the available energy in vibrational, rotational, and traslational energy. We have only performed preliminary calculations of the NO rotational distributions because at 100 K the reactivity is quite small (5%). Moreover, as there are a large number of NO vibrational levels populated, we have not enough statistics to derive rotational distributions.

Furthermore, we have seen that the temperature has an important influence in the branching ratio between both mechanisms. At 100 K the percentage of reactive trajectories corresponding to the insertion mechanism is equal to 11% of the global reactive trajectories, while at 300 K this percentage has increased to 27%. The vibrational distributions of products for both mechanisms and the global ones at 100 and 300 K are shown in Fig. 8. When the contribution of the insertion mechanism increases (at 300 K), the global vibrational distribution presents a bimodal feature. This feature is supposed to be stressed at higher temperatures when the importance of the insertion mechanism will also increase.

Table X shows the energy distribution of products from the reaction at 100 and 300 K, for both the abstraction and insertion mechanisms. At 100 K there are no differences between the energy distribution of the NO arising from the insertion and abstraction mechanisms. At 300 K the relative traslational energy in products is about 14% higher than the value at 100 K. This is due to the fact that at 300 K the products of the insertion mechanism have increased their translational energy (being in this case about 50% of the global), whereas theirvibrational and rotational energy are about 20% lower than at 100 K.

IV. SUMMARY AND CONCLUSIONS

In this work an *ab initio*, VTST, and QCT study of the $1\,^2A''$ PES implied in reaction (2) that is relevant in atmospheric chemistry has been carried out. This PES along with the $2\,^2A'$ PES studied by us in a previous paper are the most involved in the reactivity of $N(^2D)$ with O_2. We have also reported new information about excited states of NO_2 and about the existence of intersections between two PES of this system. Finally, we have calculated some properties of this reaction (rate constants and vibrational distributions of products) using an analytical representation of the $1\,^2A''$ PES obtained in this work.

The stationary points of the $1\,^2A''$ PES have been characterized at the CASSCF(17,12)/CASPT2 G2 level of theory and have shown that both the abstraction and insertion microscopic mechanisms are allowed (from an energetic point of view) through this PES. Moreover, a grid of more than 800 points has been calculated and fitted to an analytical PES. Also, two intersection seams involving the $1\,^2A''$ and $2\,^2A''$ surfaces have been studied.

As regards the kinetic calculations, the rate constant for reaction (2) through this PES has been calculated at different

TABLE X. Energy distributions of products and cross section depending on the reactants temperature and the reaction mechanism for the $1\,^2A''$ analytical PES.

	100 K ins	100 K abs	100 K total	300 K ins	300 K abs	300 K total
$\langle f'_v \rangle$	0.33	0.35	0.35	0.25	0.35	0.32
$\langle f'_r \rangle$	0.31	0.30	0.30	0.25	0.28	0.27
$\langle f'_t \rangle$	0.36	0.35	0.35	0.50	0.37	0.41
σ/Å^2	0.26±0.01	2.08±0.03	2.34±0.03	1.86±0.05	5.08±0.08	6.94±0.08

levels of theory (ICVT, ICVT/μOMT, QCT methods) obtaining, in general, small differences between them. VTST calculations including the tunnel effect show that it is not important at temperatures above 100–200 K. The global rate constant of reaction (2) has also been obtained at the QCT level, taking into account previous QCT results of our group on the $2\,^2A'$ PES and shows good agreement with the experimental values (overall note constant including physical electronic quenching).

The vibrational distributions of NO arising from the reaction at 100 K have also been calculated by means of the QCT method, showing the existence of two possible microscopic reaction mechanisms: abstraction and insertion, with different properties of products. Taking into account the previous results obtained for the $2\,^2A'$ PES, the vibrational distribution of NO arising from reaction (2) has been calculated and compared with the experimental results. The agreement between theoretical and experimental vibrational distributions is qualitative, being the experimental distribution less excited than the theoretical one. This discrepancy may be due to the approximations involved in the calculations and also to the existence of some vibrational relaxation in the measurements. Future work is necessary to determine the origin of this difference.

ACKNOWLEDGMENTS

This work has been supported by the ''Dirección General de Enseñanza Superior (Programa Sectorial de Promoción General del Conocimiento)'' of the Spanish Ministry of Education and Culture (DGES Project Ref. PB98-1209-C02-01). Financial support from the European Union (INTAS Project Ref. 99-00701 and the ''Generalitat de Catalunya'' (Autonomous Government of Catalonia) (Ref. 2000SGR 00016) is also acknowledged. One of the authors (I.M.) also thanks the ''Generalitat de Catalunya'' for a ''Beca de Formació d'Investigadors'' (Predoctoral Research Grant). The authors are also grateful to the ''Center de Computació i Comunicacions de Catalunya [C^4 (CESCA/CEPBA)]'' for providing a part of the computer time.

[1] M. González, I. Miquel, and R. Sayós, Chem. Phys. Lett. **335**, 339 (2001), and references therein.
[2] M. W. Chase, Jr., C. A. Davies, J. R. Downey, Jr., D. J. Frurip, R. A. McDonald, and A. N. Syverud, J. Phys. Chem. Ref. Data Suppl. **1**, 14 (1985).
[3] S. Baskin and J. A. Stanner, in *Atomic Energy Levels and Grotrian Diagrams 1* (North-Holland, Amsterdam, 1975), Vol. 1.
[4] F. Kaufman, ''Atmospheric reactions involving neutral constituents—An evaluation,'' paper presented at the American Geophysical Union Meeting, San Francisco, CA, December, 1968.
[5] G. Black, T. G. Slanger, G. A. St. John, and R. A. Young, J. Chem. Phys. **51**, 116 (1969).
[6] C. L. Lin and F. Kaufman, J. Chem. Phys. **55**, 3760 (1971).
[7] T. G. Slanger, B. J. Wood, and G. Black, J. Geophys. Res. **76**, 8430 (1971).
[8] D. Husain, L. J. Kirsch, and J. R. Wiesenfeld, Faraday Discuss. Chem. Soc. **53**, 201 (1972).
[9] D. Husain, S. K. Mitra, and A. N. Young, J. Chem. Soc., Faraday Trans. 2 **10**, 1721 (1974).
[10] J. E. Davenport, T. G. Slanger, and G. Black, J. Geophys. Res. **81**, 12 (1976).
[11] M. P. Iannuzzi and F. Kaufman, J. Chem. Phys. **73**, 4701 (1980).
[12] B. Fell, I. V. Rivas, and D. L. McFadden, J. Phys. Chem. **85**, 224 (1981).
[13] L. G. Piper, M. E. Donahue, and W. T. Rawlins, J. Phys. Chem. **91**, 3883 (1987).
[14] P. D. Whitefield and F. E. Hovis, Chem. Phys. Lett. **135**, 454 (1987).
[15] Y. Shihira, T. Suzuki, S. Unayuma, H. Umemoto, and S. Tsunashima, J. Chem. Soc., Faraday Trans. **90**, 549 (1994).
[16] L. E. Jusinski, G. Black, and T. G. Slanger, J. Phys. Chem. **92**, 5977 (1988).
[17] J. Herron, J. Phys. Chem. Ref. Data **28**, 1453 (1999).
[18] M. Braunstein and J. W. Duff, J. Chem. Phys. **113**, 7406 (2000).
[19] W. T. Rawlins, M. E. Fraser, and S. M. Miller, J. Phys. Chem. **93**, 1097 (1989).
[20] M. González, I. Miquel, and R. Sayós, J. Chem. Phys. **115**, 2530 (2001).
[21] B. O. Roos, P. R. Taylor, and P. E. M. Siegbahn, Chem. Phys. **48**, 157 (1980).
[22] B. O. Roos, Adv. Chem. Phys. **69**, 399 (1987).
[23] K. Andersson, Theor. Chim. Acta **91**, 31 (1995).
[24] T. H. Dunning, Jr., J. Chem. Phys. **90**, 1007 (1989).
[25] M. González, R. Valero, and R. Sayós, J. Chem. Phys. **115**, 2540 (2001).
[26] M. González, R. Valero, and R. Sayós, Chem. Phys. Lett. **343**, 119 (2001).
[27] R. González-Luque, M. Merchán, and B. O. Roos, Chem. Phys. **171**, 107 (1993).
[28] MOLCAS Version 4.1, K. Anderson, M. R. A. Blomberg, M. P. Fülscher *et al.*, Lund University, Sweden, 1998.
[29] W. C. Ermler, H. C. Hsieh, and L. B. Harding, Comput. Phys. Commun. **51**, 257 (1988).
[30] J. N. Murrell, S. Carter, S. C. Farantos, P. Huxley, and A. J. C. Varandas, *Molecular Potential Energy Surfaces* (Wiley, New York, 1984).
[31] DIATOMFIT, M. González, and R. Sayós (unpublished program).
[32] SM3FIT, R. Sayós, and M. González (unpublished program).
[33] R. Sayós, J. Hernando, J. Hijazo, and M. González, Phys. Chem. Chem. Phys. **1**, 947 (1999).
[34] M. González, J. Hernando, J. Millán, and R. Sayós, J. Chem. Phys. **110**, 7326 (1999).
[35] M. González, J. Hernando, I. Baños, and R. Sayós, J. Chem. Phys. **111**, 8913 (1999).
[36] R. Sayó, M. González, and C. Oliva, J. Chem. Phys. **113**, 6736 (2000).
[37] M. González, J. Hernando, M. P. Puyuelo, and R. Sayós, J. Chem. Phys. **113**, 6748 (2000).
[38] M. González, R. Valero, and R. Sayós, J. Chem. Phys. **113**, 10 983 (2000).
[39] R. Sayós, J. Hernando, R. Francia, and M. González, Phys. Chem. Chem. Phys. **2**, 523 (2000).
[40] D. G. Truhlar, A. D. Isaacson, and B. C. Garret, in *Theory of Chemical Reaction Dynamics*, edited by M. Baer (CRC, Boca Raton, FL, 1985), Vol. 4, p. 65.
[41] R. Steckler, Y.-Y. Chuang, E. L. Coitiño *et al.*, POLYRATE—version 7.0, University of Minnesota, Minneapolis, 1996.
[42] D. G. Truhlar and J. T. Muckerman, in *Atom–Molecule Collision Theory. A. Guide for the Experimentalist*, edited by R. B. Bernstein (Plenum, New York, 1979), Chap. 16.
[43] TRIQCT, R. Sayós, and M. González (unpublished program).
[44] H. C. Longuet-Higgings, Proc. R. Soc. London, Ser. A **344**, 147 (1975).
[45] G. J. Atchity, S. S. Xantheas, and K. Ruedenberg, J. Chem. Phys. **95**, 1862 (1991).
[46] C. F. Jackels and E. R. Davidson, J. Chem. Phys. **65**, 2941 (1976).
[47] G. D. Gillespie and A. U. Khan, J. Chem. Phys. **63**, 3425 (1975).
[48] U. Kaldor, Chem. Phys. Lett. **185**, 131 (1991).
[49] T. D. Crawford, J. F. Stanton, P. G. Szalay, and H. F. Schaefer III, J. Chem. Phys. **107**, 2525 (1997).
[50] K. Aoki, K. Hoshima, and K. Shibuya, J. Chem. Phys. **105**, 2228 (1996).
[51] K. P. Huber and G. Herzberg, in *Molecular Spectra and Molecular Structure* (Van Nostrand Reinhold, New York, 1979), Vol. 4.